Applied Catalysis B: Environmental 338 (2023) 123072

Contents lists available at ScienceDirect

Applied Catalysis B: Environmental

journal homepage: www.elsevier.com/locate/apcatb

Comparison of precursors for the synthesis of Cu-SSZ-39 zeolite catalysts for NH_3-SCR reaction

Jinpeng Du [a,b,d], Shichao Han [a,b], Chi Huang [a,c], Yulong Shan [d], Yan Zhang [a,b], Wenpo Shan [a,b,*], Hong He [a,c,d]

[a] Center for Excellence in Regional Atmospheric Environment, Institute of Urban Environment, Chinese Academy of Sciences, Xiamen 361021, China
[b] Zhejiang Key Laboratory of Urban Environmental Processes and Pollution Control, Ningbo Urban Environment Observation and Research Station, Institute of Urban Environment, Chinese Academy of Sciences, Ningbo 315800, China
[c] University of Chinese Academy of Sciences, Beijing 100049, China
[d] State Key Joint Laboratory of Environment Simulation and Pollution Control, Research Center for Eco-Environmental Sciences, Chinese Academy of Sciences, Beijing 100085, China

ARTICLE INFO

Keywords:
NH_3-SCR
Cu-SSZ-39
Precursor
Si/Al ratio
Hydrothermal stability

ABSTRACT

Cu-SSZ-39 zeolites are noted for excellent NH_3-SCR activity and hydrothermal stability for applications on diesel vehicles. In this study, Cu-SSZ-39 zeolites were prepared using four precursors. The results showed that the Cu-SSZ-39 prepared using ZSM-5 as precursor ($Cu_{2.5}$-SSZ-39-Z) has high atomic utilization and the largest particle size, comparing with those using Y, beta and colloidal silica. The Si/Al ratio of $Cu_{2.5}$-SSZ-39-Z is 9.0, and over 32% of Cu ions are $Cu(OH)^+$ species. $Cu_{2.5}$-SSZ-39-Z exhibited the best low-temperature NH_3-SCR activity and hydrothermal stability. Over 90% of NO_x conversion was achieved in the temperature range of 200–550 °C; meanwhile, over 90% NO_x conversion could be obtained between 225 °C and 450 °C after hydrothermal aging at 850 °C for 16 h or 900 °C for 5 h. The excellent activity and hydrothermal stability make ZSM-5 the preferred precursor for industrial preparation of Cu-SSZ-39 zeolite.

1. Introduction

Nitrogen oxides (NO_x) emitted from diesel vehicles are among the main precursors of particulate matter (PM) and ozone (O_3) pollution [1,2]. Selective catalytic reduction with NH_3 (NH_3-SCR) is the dominant technology for the abatement of NO_x from diesel vehicles [3,4]. Usually, a diesel particulate filter (DPF) for the removal of PM locates in front of the SCR system, and the regeneration of the DPF will expose the SCR catalyst to extremely high temperatures and humid conditions. Therefore, besides catalytic activity, hydrothermal stability is also crucial for the application of NH_3-SCR catalysts on diesel vehicles.

Cu-based small pore zeolites are known for good NH_3-SCR activity and hydrothermal stability [5–7]. Since Peden et al. firstly reported the excellent SCR performance of Cu-SSZ-13 in 2010 [8], hundreds of related papers have been published. However, Cu-SSZ-13 has difficulty enduring hydrothermal aging over 850 °C. Xiao et al. successfully synthesized high-silica Cu-ZJM-7 (KFI structure) without the use of organic templates. Over 80% of NO conversion can still be obtained from 250 to 400 °C in high-silica Cu-ZJM-7 even after hydrothermal aging at 850 °C [9]. Hong and Nam et al. developed high-silica Cu-LTA zeolites which presented outstanding hydrothermal stability. High NO_x conversion can be achieved by these catalysts even after hydrothermal aging over 900 °C [10,11]. Nevertheless, the use of fluoride is unavoidable in the synthesis process of high-silica Cu-LTA, which casts a shadow on its prospects for industrial production. Cu-SSZ-39 catalysts with the AEI structure also possess excellent hydrothermal stability. With the addition of rare-earth elements, Cu-SSZ-39 catalysts can also withstand 900 °C hydrothermal aging [12]. Considering the catalytic performance and available synthetic precursors, Cu-SSZ-39 catalysts have a bright future in industrial applications.

Precursors are one of the first things to be considered for industrial production. Conventionally, Cu-SSZ-39 zeolites are prepared using high-silica Y zeolite as the precursor [13,14]. However, the production of high-silica Y zeolite demands complicated post-treatments, which are costly and environmentally unfriendly. Xiao et al. successfully developed synthesis methods for AEI using Beta, ZSM-5, colloidal silica and

* Corresponding author at: Center for Excellence in Regional Atmospheric Environment, Institute of Urban Environment, Chinese Academy of Sciences, Xiamen 361021, China.
E-mail address: wpshan@iue.ac.cn (W. Shan).

https://doi.org/10.1016/j.apcatb.2023.123072
Received 7 April 2023; Received in revised form 2 July 2023; Accepted 5 July 2023
Available online 7 July 2023

sodium aluminate as precursors [15,16]. Furthermore, Xiao et al. traced the evolution of building units during the inter-zeolite transformation of Y, beta and ZSM-5 zeolites to AEI zeolites. It was found that the double six rings (D6R) in Y can transfer directly to AEI, while the single 4 rings (S4R) and single 6 rings (S6R) in Beta and ZSM-5 assemble together to form AEI [17]. Different inter-zeolite transformation mechanisms may influence the composition of framework atoms, which further affects the catalytic performance of catalysts.

In this study, Cu-SSZ-39 zeolites were synthesized utilizing Y, Beta, ZSM-5, colloidal silica and sodium aluminate as precursors. Both the NH_3-SCR activity and hydrothermal stability were investigated for the Cu-SSZ-39 catalysts prepared from various precursors. XRD NMR, SEM and BET were used to detect the framework and morphology of the catalysts. H_2-TPR, EPR and DRIFTS were used to analyze the Cu species in the catalysts. Furthermore, the reaction processes were also investigated by *in situ* DRIFTS experiments.

2. Experimental

2.1. Catalyst preparation

The Cu-SSZ-39 catalysts were prepared using Y (Si/Al~11), Beta (Si/Al~12), ZSM-5 (Si/Al~12) as precursors and N,N-diethyl-cis-2,6-dimethylpiperidinium hydroxide (DEDMPOH) as an organic structure directing agent (OSDA) according to procedures described in the literature [15]. For the synthesis of Cu-SSZ-39 from Y/Beta/ZSM-5, the molar composition of materials was as follows: 1.0 Y/Beta/ZSM-5: 0.17 Na_2O: 0.14 DEDMPOH: 30 H_2O: 0.017 zeolite seeds. The initial gel was sealed into autoclaves and crystallized at 140 °C for 4 days with rotation. The obtained solid was washed with de-ionized water and dried at 110 °C overnight to prepare Na-type SSZ-39 zeolites. After calcining at 600 °C for 6 h to remove the OSDA, the obtained Na-type SSZ-39 zeolites were ion-exchanged with NH_4Cl and $Cu(NO_3)_2$ solutions subsequently. After drying the samples at 110 °C overnight and calcining at 600 °C for 6 h, the final products were obtained. According to the results of ICP-OES (Table 1), the obtained catalysts were called $Cu_{2.6}$-SSZ-39-Y, $Cu_{2.6}$-SSZ-39-B and $Cu_{2.5}$-SSZ-39-Z, respectively.

For the synthesis of Cu-SSZ-39 from colloidal silica and sodium aluminate, the molar composition of the material mixture was as follows: 1.0 SiO_2: 0.017 Al_2O_3: 0.35 Na_2O: 0.12 DEDMPOH: 44 H_2O: 0.017 zeolite seeds [16]. The synthesis processes were the same as used for the Cu-SSZ-39 catalysts prepared from Y, Beta and ZSM-5. According to the results of ICP-OES (Table 1), the final product prepared by colloidal silica and sodium aluminate was named $Cu_{2.5}$-SSZ-39-C.

2.2. Characterization

Inductively coupled plasma-optical emission spectrometry (ICP-OES) was used to examine the elemental contents of catalysts, and the experiments were carried out on a PerkinElmer Optima 8300 spectrometer. X ray diffraction (XRD) was utilized to examine the crystallization of the catalysts. The experiments were conducted on a Brucker D8 Advance diffractometer with Cu Kα radiation (λ = 0.15406 nm). Scanning electron microscopy (SEM) was used to examine the morphology of the catalysts, and the experiments were carried out on a Hitachi S4800 microscope. Transmission electron microscopy (TEM) was used to detect morphological details of the aged catalysts, and the experiments were carried out on a JEM-F200 microscope. Nitrogen adsorption-desorption experiments were used to examine the surface areas and pore volumes of the catalysts, and the experiments were carried out on a Micromeritics 3Flex adsorption analyzer. Nuclear magnetic resonance (NMR) was used to detect the coordination environment of framework atoms, and experiments were conducted on a Bruker 600 M spectrometer.

Hydrogen temperature programmed reduction (H_2-TPR) experiments were carried out to detect the redox ability of the Cu-SSZ-39 catalysts. Experiments were conducted on a Micromeritics AutoChem 2920 chemisorption analyzer. The catalysts were pre-treated under 10% O_2/He at 500 °C for 1 h, and the TPR process was conducted under 10% H_2/Ar, starting at 50 °C with a ramp of 10 °C/min. Electron paramagnetic resonance (EPR) experiments were conducted on a Bruker E500 EPR spectrometer at 120 K, examining the paramagnetic Cu ions. *In situ* DRIFTS of NH_3 adsorption was utilized to detect Cu species in the catalysts. Samples were pre-treated under 20% O_2/N_2 at 500 °C for 30 min, and the adsorption of NH_3 was carried out at 25 °C under 500 ppm NH_3/N_2 until saturation. Experiments were conducted on a Thermo Nicolet IS50 spectrometer with MCT/A detector. Ammonia temperature programmed desorption (NH_3-TPD) experiments were utilized to examine the acidity of the catalysts. The catalysts were pre-treated in 20% O_2/N_2 at 500 °C for 30 min, and the adsorption process was conducted at 100 °C. The desorption process was conducted in N_2 with a total gas flow of 300 mL/min, with a ramp rate being of 10 °C/min. The outlet gas was detected by a Thermo Nicolet IS50 equipment FTIR spectrometer. X-ray photoelectron spectroscopy (XPS) was carried out to detect the atomic concentration on the surface of prepared catalysts, and the experiments were conducted on Axis Supra spectroscopy.

In situ DRIFTS experiments were used to investigate the reaction process on the catalysts, and the instrument and pretreatment process were the same as used in the NH_3 adsorption experiments. To examine the reaction between adsorbed NH_3 and gas-phase NO+O_2 at 200 °C, the catalysts were exposed to 500 ppm NH_3/N_2 until saturated, followed by the introduction of 500 ppm NO and 5% O_2. The reaction process between adsorbed nitrate species and NH_3 at 200 °C was also investigated. 500 ppm NO and 5% O_2 were introduced until saturation, followed by the introduction of 500 ppm NH_3.

2.3. NH_3-SCR activity test

NH_3-SCR activity tests were conducted in a fixed-bed reactor with the catalysts sieved to 40–60 mesh. To simulate practical diesel vehicle emissions, 500 ppm NO, 500 ppm NH_3, 5% O_2, and 5% H_2O were mixed in the inlet, with N_2 as balance gas, and the total gas flow was 500 mL/min with a GHSV of 200,000 h^{-1}. The outlet gas was detected by an online infrared spectrometer (Thermo Nicolet IS50). NO_x conversion was calculated by the following equation:

$$NO_x \quad conversion = \left(1 - \frac{[NO_x]_{out}}{[NO_x]_{in}}\right) \times 100\% (\mathrm{NOx} = \mathrm{NO} + \mathrm{NO2})$$

Hydrothermal aging treatments were also carried out in a fixed-bed reactor. 200 mg sieved catalysts (40–60 mesh) were treated with 10% H_2O/air with total gas flow of 200 mL/min. The catalysts aged at 850 °C for 16 h were named: $Cu_{2.6}$-SSZ-39-Y-HTA850, $Cu_{2.6}$-SSZ-39-B-HTA850, $Cu_{2.5}$-SSZ-39-Z-HTA850 and $Cu_{2.5}$-SSZ-39-C-HTA850, respectively. For the catalysts aged at 900 °C for 5 h, they were named as: $Cu_{2.6}$-SSZ-39-Y-HTA900, $Cu_{2.6}$-SSZ-39-B-HTA900, $Cu_{2.5}$-SSZ-39-Z-HTA900, and $Cu_{2.5}$-SSZ-39-C-HTA900, respectively.

SO_2 resistance tests were carried out with the fresh Cu-SSZ-39 catalysts being sulfated under 100 ppm NH_3 at 400 °C for 5 h. The regeneration was conducted under 10% H_2O/ air at 800 °C for 2 h.

Table 1
Elemental composition of the fresh Cu-SSZ-39 catalysts (ICP-OES).

	Cu	Si	Al	Si/Al	Cu/Al
$Cu_{2.6}$-SSZ-39-Y	2.6	32.3	4.3	7.2	0.25
$Cu_{2.6}$-SSZ-39-B	2.6	35.0	3.9	8.6	0.28
$Cu_{2.5}$-SSZ-39-Z	2.5	33.3	3.6	9.0	0.30
$Cu_{2.5}$-SSZ-39-C	2.5	32.4	4.7	6.7	0.23

3. Results

3.1. NH_3-SCR activity and hydrothermal stability

The NH_3-SCR activity and hydrothermal stability of the Cu-SSZ-39 catalysts prepared from different precursors are illustrated in Fig. 1. All the fresh catalysts possessed good catalytic activity, with over 90% NO_x conversion from 225 °C to 550 °C. Among them, the temperature window of 90% NO_x conversion for $Cu_{2.5}$-SSZ-39-Z was 200–550 °C, and over 94% of NO_x could be converted at 200 °C. NO_x conversion below 200 °C followed the order: $Cu_{2.5}$-SSZ-39-Z > $Cu_{2.6}$-SSZ-39-B > $Cu_{2.6}$-SSZ-39-Y > $Cu_{2.5}$-SSZ-39-C.

After hydrothermal aging at 850 °C, all the catalysts showed a decrease in catalytic activity; nevertheless, over 80% NO_x conversion could still be obtained from 225 °C to 500 °C. Meanwhile, $Cu_{2.5}$-SSZ-39-Z-HTA850 exhibited over 90% NO_x conversion between 225 and 450 °C. After hydrothermal aging at 900 °C, the prepared catalysts presented diverse catalytic performance. In the whole temperature range, NO_x conversion of the catalysts followed the order: $Cu_{2.5}$-SSZ-39-Z-HTA900 > $Cu_{2.6}$-SSZ-39-B-HTA900 > $Cu_{2.5}$-SSZ-39-C-HTA900 > $Cu_{2.6}$-SSZ-39-Y-HTA900. The temperature window of 90% NO_x conversion for $Cu_{2.5}$-SSZ-39-Z-HTA900 was 225–450 °C, which is comparable to that of $Cu_{2.5}$-SSZ-39-Z-HTA850. Overall, it was clearly shown that the Cu-SSZ-39 catalyst prepared using ZSM-5 as precursor possesses the best low-temperature NH_3-SCR activity and hydrothermal stability.

N_2O is one of the greenhouse gases, therefore, the formation of N_2O during NH_3-SCR should be noted. N_2O was mainly generated in two temperature ranges: around 250 °C and over 450 °C. The N_2O formed at low and high temperatures are mainly due to the decomposition of NH_4NO_3 and the non-selective oxidation of NH_3, respectively. As can be seen in Fig. S2, for the fresh catalysts, hardly any difference in N_2O formation can be observed among all the four catalysts. Meanwhile, the concentration of N_2O was below 4.5 ppm for all the four fresh catalysts, indicating their high N_2 selectivity. Little difference was also observed for the catalysts aged at 850 °C, however, more N_2O was formed over 450 °C, probably due to the non-selective oxidation of NH_3 by Cu_xO_y species. After hydrothermal aging at 900 °C, high concentration of N_2O was formed over $Cu_{2.6}$-SSZ-39-Y-A900, $Cu_{2.6}$-SSZ-39-B-A900 and $Cu_{2.5}$-SSZ-39-C-A900 around 300 °C. However, the N_2O formation of $Cu_{2.5}$-SSZ-39-Z-A900 was comparable to that of $Cu_{2.5}$-SSZ-39-Z-A850, indicating it possessed relatively good N_2 selectivity.

In our previous study, we investigated the influence of SO_2 on Cu-SSZ-39 catalyst by exposing to SO_2 at different temperatures. It turns out that the most amount of $CuSO_4$ species formed when sulfating at 400 °C, and it would be hard for Cu ions to recover after regenerating at 600 °C [18]. Therefore, in this study we discussed the influence of the prepared Cu-SSZ-39 catalysts after sulfating at 400 °C. As can be seen in Fig. S3 (a), a decrease of NO_x conversion can be seen for all the catalysts below 300 °C, comparing with the fresh catalysts. According to our previous study, the decrease of NO_x conversion was mainly due to the formation of H_2SO_4 and $CuSO_4$ species. $CuSO_4$ species cannot be fully decomposed at 600 °C [18], thus the regeneration treatments were carried out at 800 °C for 2 h. As can be seen in Fig. S3 (b), the NO_x conversion can be recovered significantly after regeneration, though a little lower than the fresh state. In conclusion, NO_x conversion was affected by the existence of SO_2, however, the activity can be almost recovered after regeneration at 800 °C. Considering NH_3-SCR catalysts are frequently exposed to high temperatures in the practical application, the Cu-SSZ-39 catalyst prepared in this study can be potentially used even SO_2 is inevitable.

3.2. Catalyst characterization

The elemental composition of the fresh catalysts was examined by ICP-OES, and the results are shown in Table 1. The Cu contents of the four fresh Cu-SSZ-39 catalysts are similar, at around 2.5–2.6 wt%. On the other hand, the Si/Al ratios of these catalysts are different from each other, following the order: $Cu_{2.5}$-SSZ-39-Z (9.0) > $Cu_{2.6}$-SSZ-39-B (8.6) > $Cu_{2.6}$-SSZ-39-Y (7.2) > $Cu_{2.5}$-SSZ-39-C (6.7). The XRD patterns of the fresh and aged Cu-SSZ-39 catalysts are shown in Fig. 2. All fresh catalysts exhibit pure-phase AEI structure diffraction peaks with good crystallinity. Meanwhile, no diffraction peak for CuO species can be observed for any of the catalysts, indicating that no bulk CuO species existed. To calculate the change in relative crystallinity for the aged catalysts, the peak intensities at 17.4∘, 20.8∘, 21.5∘, 24.1∘, and 31.4∘ were integrated and compared with those of the fresh catalysts [19,20]. After hydrothermal aging at 850 °C, 74.5%, 86.7%, 82.5% and 74.9% relative crystallinity was maintained for $Cu_{2.6}$-SSZ-39-Y-HTA850, $Cu_{2.6}$-SSZ-39-B-HTA850, $Cu_{2.5}$-SSZ-39-Z-HTA 850 and $Cu_{2.5}$-SSZ-39-C-HTA850, respectively. Cu-SSZ-39 catalysts prepared with Beta and ZSM-5 as precursors maintained higher crystallinity, probably due to their higher Si/Al ratios [21,22]. In addition, $Cu_{2.6}$-SSZ-39-Y-HTA900, $Cu_{2.6}$-SSZ-39-B-HTA900 and $Cu_{2.5}$-SSZ-39-C-HTA900 presented amorphous phases, indicating the collapse of the framework. Among these three catalysts, $Cu_{2.6}$-SSZ-39-B-HTA900 maintained a weak diffraction peak around 9.7 °, indicating that its framework was a bit more stable. Surprisingly, 82.8% relative crystallinity was maintained for $Cu_{2.5}$-SSZ-39-Z-HTA900, indicating that its framework can even survive 900 °C hydrothermal aging.

To determine the coordination environment of the framework atoms, ^{27}Al NMR and ^{29}Si NMR were used. As shown in Fig. 3, the peaks with chemical shifts around 58 ppm were attributed to tetracoordinated framework Al atoms, and the peaks around 0 ppm were assigned to hexacoordinated extra-framework Al atoms [23,24]. It is hard to see any signal of extra-framework Al atoms for the fresh Cu-SSZ-39 catalysts, indicating that all the fresh catalysts were well crystallized. The results of ^{29}Si NMR experiments are shown in Fig. S4. Peaks around − 112 ppm

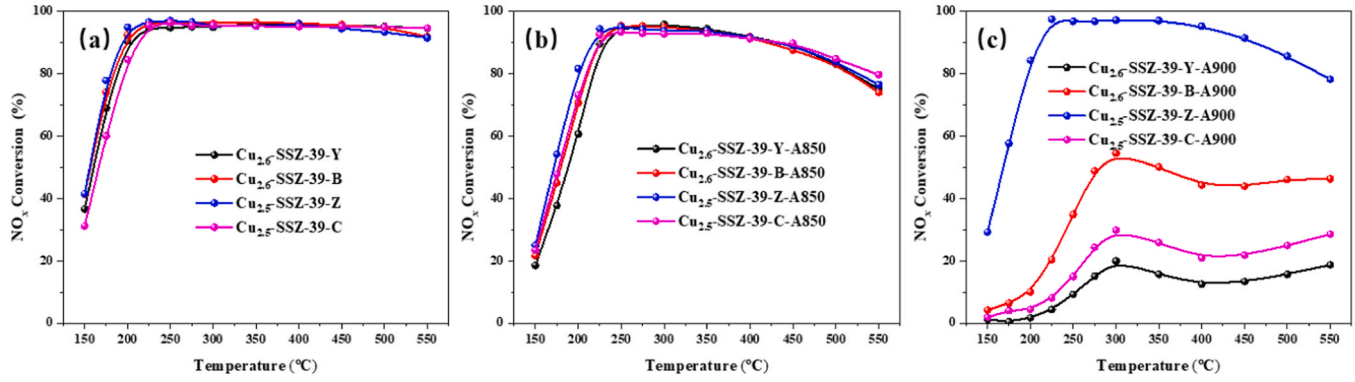

Fig. 1. NH_3-SCR activity of (a) fresh Cu-SSZ-39 catalysts, (b) Cu-SSZ-39 catalysts after hydrothermal aging at 850 °C, and (c) Cu-SSZ-39 catalysts after hydrothermal aging at 900 °C.

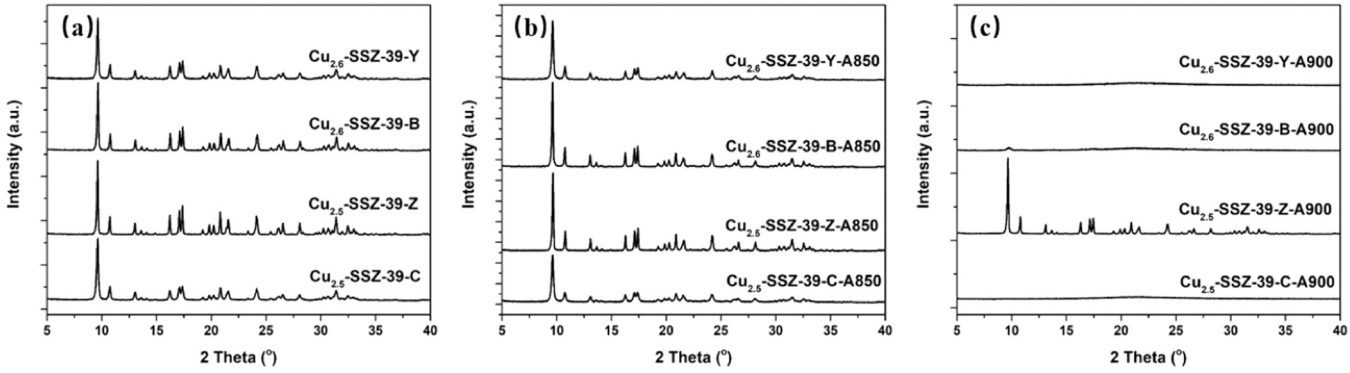

Fig. 2. XRD patterns of (a) fresh Cu-SSZ-39 catalysts, (b) Cu-SSZ-39 catalysts after hydrothermal aging at 850 °C, and (c) Cu-SSZ-39 catalysts after hydrothermal aging at 900 °C.

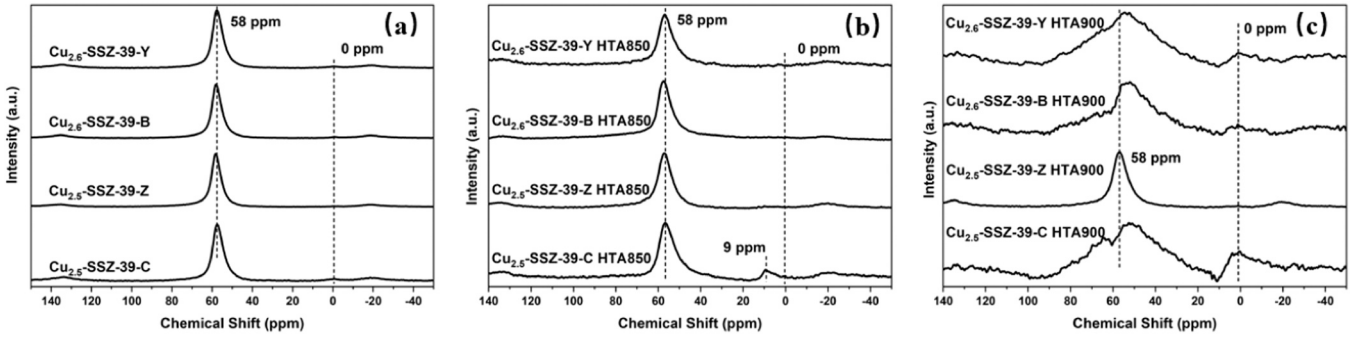

Fig. 3. ^{27}Al NMR profiles of (a) fresh Cu-SSZ-39 catalysts, (b) Cu-SSZ-39 catalysts after hydrothermal aging at 850 °C, and (c) Cu-SSZ-39 catalysts after hydrothermal aging at 900 °C.

were assigned to the Si atoms with 4 Si atoms coordinated, and peaks around − 106 ppm were attributed to the Si atoms coordinated with 1 Al and 3 Si atoms [12,23]. $Cu_{2.6}$-SSZ-39-B and $Cu_{2.5}$-SSZ-39-Z possess less Si(1Al3Si) atoms; thus, their Si/Al ratios were higher. After hydrothermal aging at 850 °C, only a weak peak around 9 ppm can be observed for $Cu_{2.5}$-SSZ-39-C HTA850 in ^{27}Al NMR spectra. However, the contents of

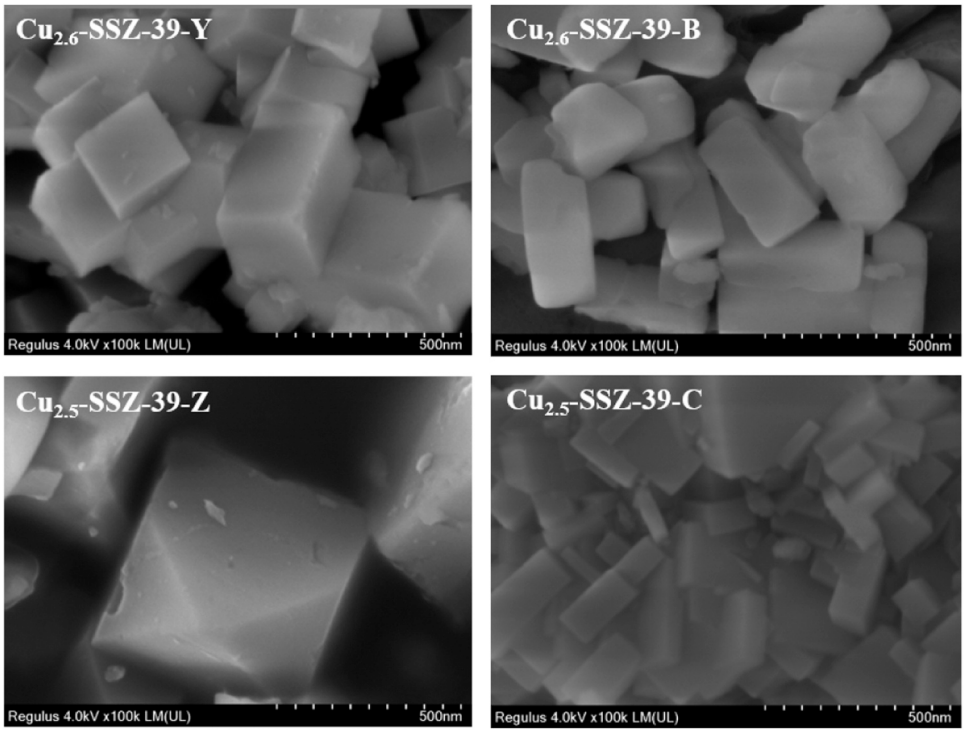

Fig. 4. SEM images of fresh Cu-SSZ-39 catalysts.

Si(1Al3Si) atoms decreased for all four catalysts compared with the fresh catalysts, according to the ^{29}Si NMR spectra. This indicates that dealumination occurred for these catalysts after hydrothermal aging at 850 °C, and the absence of a signal at 0 ppm in the ^{27}Al NMR spectra is probably due to the paramagnetic effect of Cu ions [25,26]. After hydrothermal aging at 900 °C, unlike $Cu_{2.5}$-SSZ-39-Z HTA900, the ^{27}Al and ^{29}Si NMR spectra of the other three catalysts were notably broadened, indicating serious dealumination [27,28]. Combined with the XRD results, these data showed that the framework of $Cu_{2.6}$-SSZ-39-Y-HTA900 and $Cu_{2.5}$-SSZ-39-C-HTA900 collapsed completely, and the framework of $Cu_{2.6}$-SSZ-39-B-HTA900 mostly collapsed.

The morphologies of the prepared catalysts were explored by SEM, and the results are shown in Fig. 4. $Cu_{2.6}$-SSZ-39-Y and $Cu_{2.6}$-SSZ-39-B show similar cubic morphologies with particle size around 100–300 nm. $Cu_{2.5}$-SSZ-39-Z presents octahedral shaped particles with size around 500 nm, which is the largest among the prepared catalysts. Generally, the larger the particle size, the better the crystallinity of the catalyst, which is in accordance with the XRD results showing that the peak intensity of $Cu_{2.5}$-SSZ-39-Z was higher than those of the other catalysts. $Cu_{2.5}$-SSZ-39-C has a cubic shape with particle size between 50 and 200 nm, which is the smallest among the catalysts, corresponding to the lowest XRD peak intensity.

The SEM images of Cu-SSZ-39 catalysts hydrothermally aged at 850 °C and 900 °C are shown in Fig. S5. Compared with the fresh catalysts, little change in morphology can be observed for the catalysts aged at 850 °C or 900 °C. However, the TEM images of the 900 °C aged catalysts (presented in Fig. S6) show that mesopores exist in the particles of $Cu_{2.6}$-SSZ-39-Y-HTA900, $Cu_{2.6}$-SSZ-39-B-HTA900 and $Cu_{2.5}$-SSZ-39-C-HTA900. Combining the results of XRD and NMR, unlike $Cu_{2.5}$-SSZ-39-Z-HTA900, the framework of the other catalysts collapsed after aging at 900 °C, forming mesopores.

N_2 adsorption-desorption experiments were carried out to measure the surface area and pore volume of the fresh and aged catalysts, and the results are shown in Table 2. The specific surface areas of all the fresh catalysts are around 749–793 m^2/g, and the pore volumes are around 0.27–0.29 cm^3/g. The approximately equal specific surface areas and pore volumes indicate that all four fresh catalysts possess good pore structures. After hydrothermal aging at 850 °C, significant decreases in surface area and pore volume can be observed for $Cu_{2.6}$-SSZ-39-Y-HTA850 and $Cu_{2.5}$-SSZ-39-C-HTA850, while $Cu_{2.5}$-SSZ-39-Z-HTA850 maintained the highest surface area and pore volume, indicating the high stability of this catalyst. After hydrothermal aging at 900 °C, the surface area and pore volume of $Cu_{2.6}$-SSZ-39-Y-HTA900 and $Cu_{2.5}$-SSZ-39-C-HTA900 decreased sharply, and $Cu_{2.6}$-SSZ-39-B-HTA900 only maintained 73 m^2/g surface area and 0.02 cm^3/g pore volume. The collapse of the framework and formation of mesopores significantly affected the surface areas and pore volumes of these three catalysts. It worth noting that $Cu_{2.5}$-SSZ-39-Z-HTA900 maintained a surface area of 637 m^2/g and pore volume of 0.24 cm^3/g, indicating that the framework and pores of Cu-SSZ-39 prepared from ZSM-5 possess excellent hydrothermal stability.

Table 2
Specific surface area and pore volume of all the catalysts (N_2 adsorption-desorption experiment).

	Surface area (m^2/g)	Pore volume (cm^3/g)
$Cu_{2.6}$-SSZ-39-Y	749	0.28
$Cu_{2.6}$-SSZ-39-B	763	0.28
$Cu_{2.5}$-SSZ-39-Z	793	0.29
$Cu_{2.5}$-SSZ-39-C	757	0.27
$Cu_{2.6}$-SSZ-39-Y-HTA850	557	0.20
$Cu_{2.6}$-SSZ-39-B-HTA850	646	0.24
$Cu_{2.5}$-SSZ-39-Z-HTA850	713	0.27
$Cu_{2.5}$-SSZ-39-C-HTA850	572	0.20
$Cu_{2.6}$-SSZ-39-Y-HTA900	23	0.001
$Cu_{2.6}$-SSZ-39-B-HTA900	73	0.02
$Cu_{2.5}$-SSZ-39-Z-HTA900	637	0.24
$Cu_{2.5}$-SSZ-39-C-HTA900	39	0.01

3.3. Characterization of Cu species

H_2-TPR profiles of the prepared Cu-SSZ-39 catalysts are shown in Fig. 4. Peak A and peak B were attributed to the reduction of $Cu(OH)^+$ and Cu^{2+} species to Cu^+, respectively [29]. Peak C was assigned to the reduction of Cu^+ to Cu^0, and appeared over 950 °C for the fresh catalysts [30]. It is evident that $Cu_{2.6}$-SSZ-39-B and $Cu_{2.5}$-SSZ-39-Z contained more $Cu(OH)^+$ species, which could have been due to the higher Si/Al ratio [31]. Moreover, the reduction peak for $Cu(OH)^+$ species in $Cu_{2.6}$-SSZ-39-Y and $Cu_{2.5}$-SSZ-39-C are overlapped by the reduction peak of Cu^{2+}. $Cu(OH)^+$ species possess better low-temperature NH_3-SCR activity [32,33]; thus, $Cu_{2.6}$-SSZ-39-B and $Cu_{2.5}$-SSZ-39-Z showed higher NO_x conversion at low temperature.

After hydrothermal aging at 850 °C, the reduction peaks for $Cu(OH)^+$ species weakened remarkably for $Cu_{2.6}$-SSZ-39-B-HTA850 and $Cu_{2.5}$-SSZ-39-Z-HTA-850. Some of the $Cu(OH)^+$ species might be transformed into Cu^{2+} species or Cu_xO_y species [34]. Moreover, the reduction of Cu^+ species for all the Cu-SSZ-39 catalysts moved to lower temperatures, which indicates that the coordination of Cu ions to framework atoms was weakened, due to the damage to the framework [35]. Nevertheless, the reduction temperature of Cu^+ to Cu^0 in $Cu_{2.5}$-SSZ-39-Z-HTA-850 was the highest, indicating that its framework is the most stable.

After hydrothermal aging at 900 °C, peak D, corresponding to the reduction of Cu^{2+} in $CuAlO_x$, emerged for $Cu_{2.6}$-SSZ-39-Y-HTA900 and $Cu_{2.5}$-SSZ-39-C-HTA-900 [35]. Meanwhile, the reduction of Cu^+ to Cu^0 for $Cu_{2.6}$-SSZ-39-Y-HTA900 and $Cu_{2.5}$-SSZ-39-C-HTA-900 moved to about 550 °C, indicating the complete deterioration of the framework and formation of $CuAlO_x$ species [36]. The decrease in the number of SCR-active Cu^{2+} species and the collapse of the framework resulted in a dramatic decrease in NH_3-SCR activity. Peak E, attributing to the reduction of Cu_xO_y species emerged in $Cu_{2.6}$-SSZ-39-B-HTA900 and $Cu_{2.5}$-SSZ-39-C-HTA-900. In order to avoid visual errors, we made the baselines of the two curves coincide. As can be seen in Fig. S7. The reduction of Cu_xO_y species may be overlapped in peak B, therefore, the peak C which are assigned to the reduction of Cu^+ to Cu^0 can be taken for reference. The reduction of Cu^+ to Cu^0 is the second step that $Cu(OH)^+$ or Cu^{2+} being reduced to Cu^+, meanwhile, Cu_xO_y species are reduced to Cu^0 in only one step. Higher peak intensity of peak C for $Cu_{2.5}$-SSZ-39-Z-A900 than that for $Cu_{2.6}$-SSZ-39-B-A900 indicates that more $Cu(OH)^+$ /Cu^{2+} species were maintained in $Cu_{2.5}$-SSZ-39-Z-A900, while a large amount of Cu_xO_y species existed in $Cu_{2.6}$-SSZ-39-B-A900. This conclusion is in accordance with the result of EPR that more divalent Cu ions exist in $Cu_{2.5}$-SSZ-39-Z-A900 than $Cu_{2.6}$-SSZ-39-B-A900. Meanwhile, the reduction of Cu^+ moved to around 600–700 °C in $Cu_{2.6}$-SSZ-39-B-A900, indicating the damage of framework. Nevertheless, the decline in Cu^{2+} species and the shift of the Cu^+ peak was not as serious as for $Cu_{2.6}$-SSZ-39-Y-HTA900 and $Cu_{2.5}$-SSZ-39-C-HTA-900. Therefore, $Cu_{2.6}$-SSZ-39-B-HTA900 behaved a bit better in NH_3-SCR testing. $Cu_{2.5}$-SSZ-39-Z-HTA-900 maintained the highest amount of active Cu ions. Compared with $Cu_{2.5}$-SSZ-39-Z-HTA-850, little change emerged in the H_2-TPR profile of $Cu_{2.5}$-SSZ-39-Z-HTA-900, which indicates that Cu species are more stable in $Cu_{2.5}$-SSZ-39-Z-HTA-900. Therefore, high NO_x conversion was still maintained.

EPR experiments were carried out to detect paramagnetic divalent Cu ions in the fresh and aged catalysts, and the results are shown in Fig. 6. Only one spectral feature (α Cu: $g_{||}$=2.40, $A_{||}$=132/130 G) was observed for the fresh and 850 °C-aged catalysts, which was assigned to SCR-active divalent Cu ions, including Cu^{2+} and Cu $(OH)^+$ species. Besides α Cu species, another spectral feature with $g_{||}$= 2.33 and $A_{||}$= 157 G was also observed for the 900 °C-aged catalysts, corresponding to $CuAlO_x$ species [35,37].

To quantify the amount of Cu ions in all the prepared catalysts, the

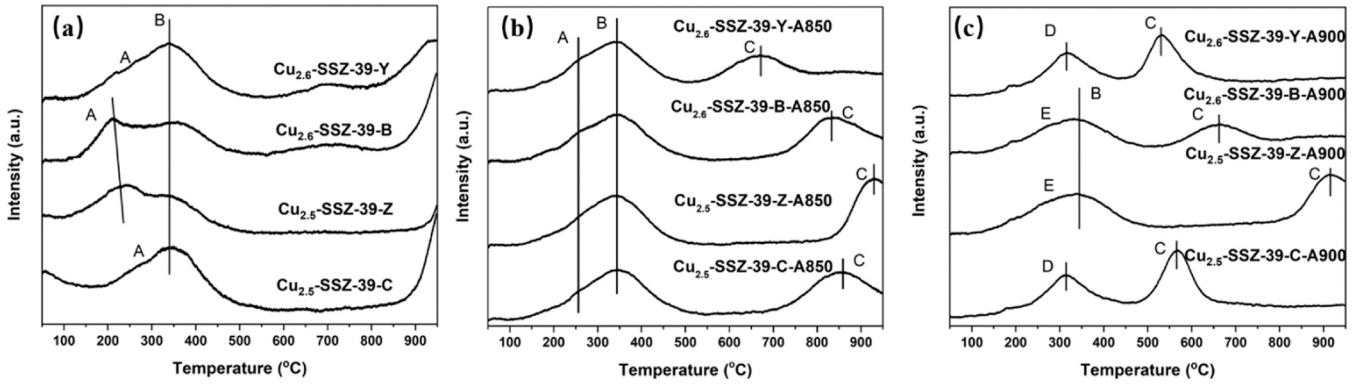

Fig. 5. H_2-TPR profiles of (a) fresh Cu-SSZ-39 catalysts, (b) Cu-SSZ-39 catalysts aged at 850 °C, and (c) Cu-SSZ-39 catalysts aged at 900 °C.

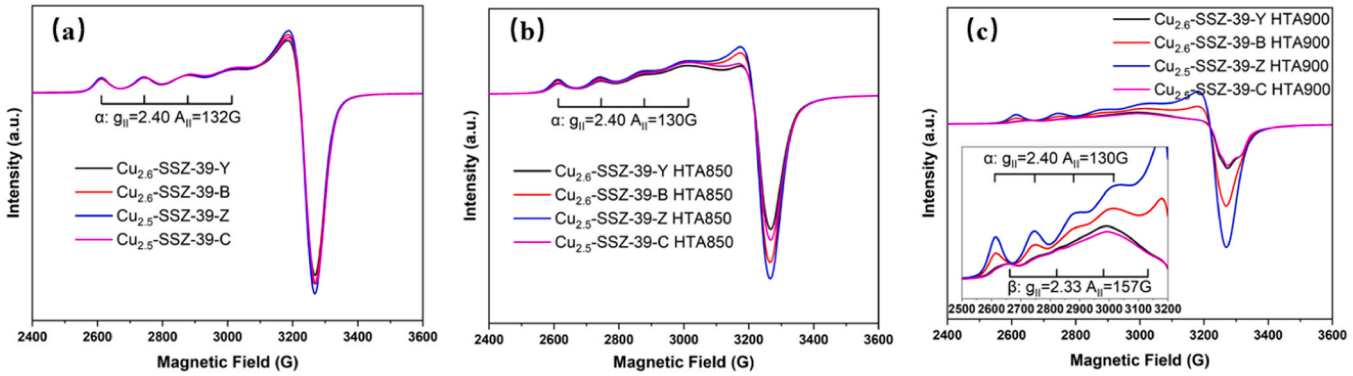

Fig. 6. EPR spectra of (a) fresh Cu-SSZ-39 catalysts, (b) Cu-SSZ-39 catalysts aged at 850 °C, and (c) Cu-SSZ-39 catalysts aged at 900 °C.

relative Cu contents of the catalysts were calculated and summarized in Fig. S8. The amounts of SCR-active divalent Cu ions in the fresh Cu-SSZ-39 catalysts are similar, which is in accordance with the ICP-OES results. After hydrothermal aging at 850 °C, the amount of SCR-active divalent Cu ions decreased in all four catalysts. The amount of Cu ions followed the order: $Cu_{2.5}$-SSZ-39-Z-HTA850 > $Cu_{2.6}$-SSZ-39-B-HTA850 > $Cu_{2.5}$-SSZ-39-C-HTA850 > $Cu_{2.6}$-SSZ-39-Y-HTA850, which follows the same order as the NH_3-SCR activity.

After hydrothermal aging at 900 °C, further decreases in the number of divalent Cu ions can be observed. $Cu_{2.5}$-SSZ-39-Z-HTA900 still possessed the highest amount of Cu ions, with 72.4% of relative Cu content maintained. Meanwhile, β Cu of $CuAlO_x$ species emerged in $Cu_{2.5}$-SSZ-39-C-HTA900 and $Cu_{2.6}$-SSZ-39-Y-HTA900, indicating the collapse of the framework of these two catalysts [35]. It is worth mentioning that no $CuAlO_x$ species emerged in $Cu_{2.6}$-SSZ-39-B-HTA900, although its framework also collapsed. 57% of SCR-active divalent Cu ions were maintained in $Cu_{2.6}$-SSZ-39-B-HTA900; thus, it performed better than $Cu_{2.5}$-SSZ-39-C-HTA900 and $Cu_{2.6}$-SSZ-39-Y-HTA900.

The interaction between Cu ions and the framework atoms induces IR absorption peaks around 950–900 cm^{-1}. In the process of NH_3 adsorption, the Cu ions complex with NH_3, and the interaction with the framework atoms weakens; thus, negative peaks emerged. The negative peaks around 900 cm^{-1} were attributed to the Cu^{2+} located near D6R, while the negative peaks around 940 cm^{-1} were assigned to $Cu(OH)^+$ species near eight member rings [38–40]. As presented in Fig. 5(a), 32.1% of the Cu ions in $Cu_{2.5}$-SSZ-39-Z are $Cu(OH)^+$ species, which is the highest among the fresh catalysts. $Cu_{2.6}$-SSZ-39-B possesses nearly 28.7% $Cu(OH)^+$ species, more than the other two catalysts. This result is in accordance with the H_2-TPR profiles showing that $Cu_{2.5}$-SSZ-39-Z and $Cu_{2.6}$-SSZ-39-B contain more $Cu(OH)^+$ species, probably due to their higher Si/Al ratio. After hydrothermal aging at 850 °C, there is a decrease in the number of $Cu(OH)^+$ species in $Cu_{2.5}$-SSZ-39-Z and $Cu_{2.6}$-SSZ-39-B, which is in accordance with the H_2-TPR results. Under this circumstance, the proportions of $Cu(OH)^+$ species among the four catalysts are similar. However, the EPR results indicate that more Cu ions exist in $Cu_{2.6}$-SSZ-39-B-HTA850 and $Cu_{2.5}$-SSZ-39-Z-HTA850. After hydrothermal aging at 900 °C, Cu^{2+} and $Cu(OH)^+$ species disappeared and only $CuAlO_x$ species remained in $Cu_{2.6}$-SSZ-39-Y-HTA900 and $Cu_{2.5}$-SSZ-39-C-HTA900; thus, hardly any peak can be seen for them. A faint negative peak at 900–950 cm^{-1} can be observed in the spectrum of $Cu_{2.6}$-SSZ-39-B-HTA900, indicating that Cu^{2+} species still existed. Moreover, the greatest amount of Cu^{2+} and $Cu(OH)^+$ species are maintained in $Cu_{2.5}$-SSZ-39-Z-HTA900, and the amount and proportion of Cu species were similar to those in $Cu_{2.5}$-SSZ-39-Z-HTA850. Therefore, $Cu_{2.5}$-SSZ-39-Z-HTA900 still exhibits high NO_x conversion, without any notable decrease compared with $Cu_{2.5}$-SSZ-39-Z-HTA850. .

3.4. Characterization of acid sites

NH_3-TPD experiments were carried out to examine the amount and strength of acid sites on the catalysts, and the results are shown in Fig. 8. Peak A is assigned to weak acid sites, which are mainly terminal hydroxyl species; Peak B is attributed to medium acid sites, which are Lewis acid sites derived from Cu^{2+} species; Peak C belongs to strong acid sites, and these are Brønsted acid sites that originate from framework Al [34,41]. To quantity the amount of acid sites, the acidity of fresh and aged catalysts was calculated and summarized in Fig. S9. The amounts of medium (Lewis) acid sites for different fresh catalysts are similar, in accordance with the EPR results that they contain similar amounts of Cu ions. However, $Cu_{2.6}$-SSZ-39-B and $Cu_{2.5}$-SSZ-39-Z contain more strong (Brønsted) acid sites.

After hydrothermal aging at 850 °C, significant decreases in Lewis acid sites and Brønsted acid sites can be observed for all the catalysts, and the desorption of NH_3 also moved to lower temperature [27,42].

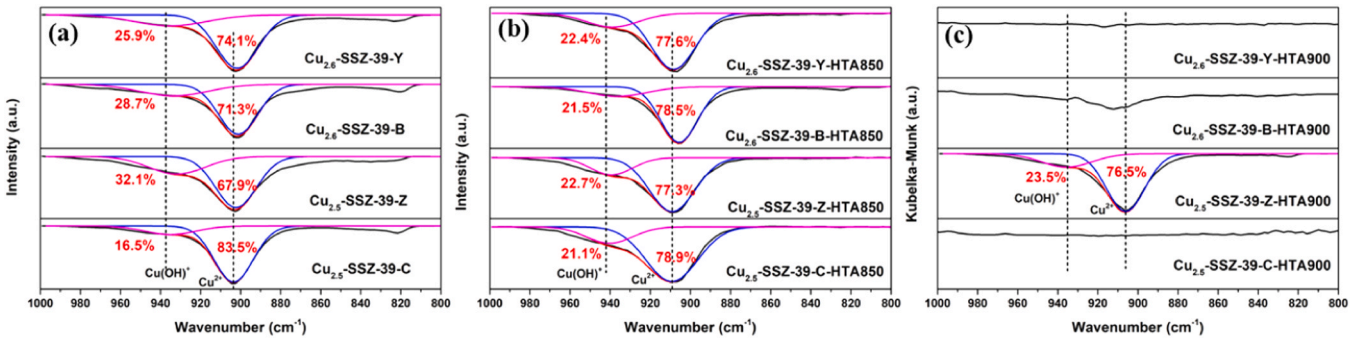

Fig. 7. *In situ* DRIFTS of NH_3 adsorption of (a) fresh Cu-SSZ-39 catalysts, (b) Cu-SSZ-39 catalysts aged at 850 °C, and (c) Cu-SSZ-39 catalysts aged at 900 °C.

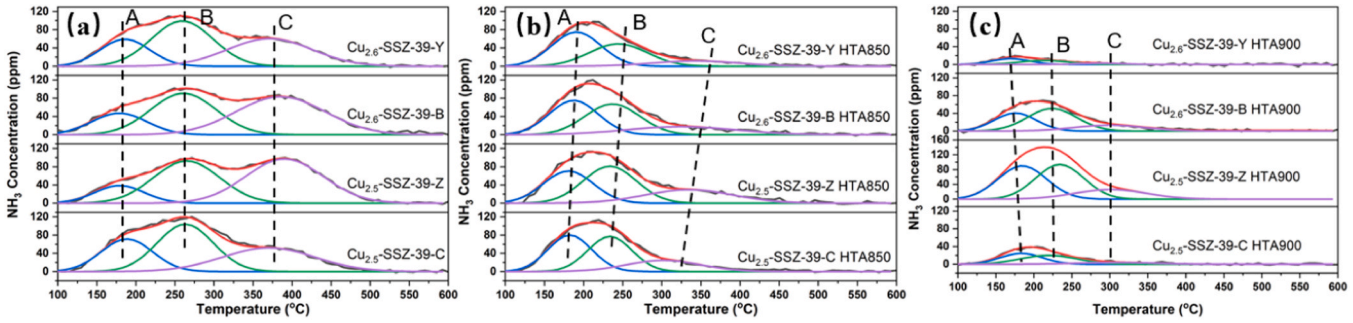

Fig. 8. NH_3-TPD profiles of (a) fresh Cu-SSZ-39 catalysts, (b) Cu-SSZ-39 catalysts aged at 850 °C, and (c) Cu-SSZ-39 catalysts aged at 900 °C.

The decrease in Lewis acid sites is due to the loss of Cu^{2+} ions, which can be proved by the EPR results. The decrease in Brønsted acid sites is due to the deterioration of the framework, which is in accordance with the XRD and NMR results. It worth mentioning that $Cu_{2.5}$-SSZ-39-Z-HTA850 still maintained the most amount of Lewis acid sites and Brønsted acid sites.

After hydrothermal aging at 900 °C, the acid sites decreased significantly for $Cu_{2.6}$-SSZ-39-Y-HTA900 and $Cu_{2.5}$-SSZ-39-C-HTA900. The loss of Lewis acid sites is associated with the decrease in the number of $Cu(OH)^+$ /Cu^{2+} species and formation of $CuAlO_x$ species. The decline in Brønsted acid sites is due to the collapse of the framework. It worth mentioning that $Cu_{2.5}$-SSZ-39-Z-HTA900 still maintained the greatest amount of Lewis and Brønsted acid sites, therefore, high NO_x conversion was maintained.

3.5. Reaction process

Y zeolites are common precursors for the synthesis of Cu-SSZ-39, while the Cu-SSZ-39 prepared from ZSM-5 exhibited the best low-temperature NH_3-SCR activity and hydrothermal stability in this study. Therefore, the reaction processes of $Cu_{2.6}$-SSZ-39-Y and $Cu_{2.5}$-SSZ-39-Z at 200 °C were compared by *in situ* DRIFTS. First, the reaction process between adsorbed NH_3 and NO+O_2 was investigated, and the spectra are shown in Fig. 9(a) and (c), respectively. The peaks at 1622 and 1624 cm^{-1} are assigned to NH_3 adsorbed on Lewis acid sites, and those at 1446 and 1452 cm^{-1} are attributed to NH_3 adsorbed on Brønsted acid sites [43]. With the introduction of NO+O_2, the peaks for NH_3 adsorbed on Lewis acid sites and Brønsted acid sites decreased simultaneously. To compare the consumption rates of NH_3 on different acid sites in $Cu_{2.6}$-SSZ-39-Y and $Cu_{2.5}$-SSZ-39-Z, the time evolution of peak intensity is summarized in Fig. S10. The consumption of NH_3 adsorbed on Lewis acid sites was faster for $Cu_{2.5}$-SSZ-39-Z in the first 8 min. This is in accordance with the NH_3-SCR activity results wherein the NO_x conversion of $Cu_{2.5}$-SSZ-39-Z is higher than that of $Cu_{2.6}$-SSZ-39-Y at 200 °C. It worth noting that the peak intensity of NH_3 adsorbed at Brønsted acid sites increased in the first several minutes. This is due to the formation of NH_4NO_3 when NO and O_2 were introduced, causing the elevation of NH_4^+, and more NH_4NO_3 species emerged in $Cu_{2.5}$-SSZ-39-Z [44]. Brønsted acid sites usually act as an NH_3 reservoir [45], and they do not participate in NH_3-SCR reaction directly. Therefore, although the consumption of NH_3 adsorbed at Brønsted acid sites was faster in $Cu_{2.6}$-SSZ-39-Y, it did not change the fact that $Cu_{2.5}$-SSZ-39-Z exhibited higher NO_x conversion.

To investigate the reaction process between nitrate species and NH_3, the catalysts were first exposed to NO and O_2 until saturated, and then NH_3 was introduced at 0 min. The peaks around 1650–1550 cm^{-1} at 0 min were assigned to nitrate species adsorbed on Cu ions [46]. More Cu-NO_3^- species existed in $Cu_{2.5}$-SSZ-39-Z compared with $Cu_{2.6}$-SSZ-39-Y. As mentioned above, $Cu_{2.5}$-SSZ-39-Z possessed more Cu $(OH)^+$ species than $Cu_{2.6}$-SSZ-39-Y. $Cu(OH)^+$ species presented higher redox ability than Cu^{2+} species; therefore, Cu-NO_3^- species formed more easily in $Cu_{2.5}$-SSZ-39-Z. As shown in Fig. S10, more NH_4NO_3 species formed in $Cu_{2.5}$-SSZ-39-Z, which is also due to its high redox ability. Cu-NO_3^- species can be consumed rapidly with the introduction of NH_3. However, from 2 to 3 min on, the peaks of NH_3 adsorbed at Brønsted acid site emerged and obscured the adsorption peak of Cu-NO_3^- at 1624 cm^{-1}. Therefore, it is more accurate to observe the changes in the peaks at 1593 and 1574 cm^{-1}. It is clear that these two peaks disappeared in the 4th minute, indicating that Cu-NO_3^- species are very SCR-active. Cu-NO_3^- species are more easily formed in $Cu_{2.5}$-SSZ-39-Z; therefore, it presented better SCR activity than $Cu_{2.6}$-SSZ-39-Y.

4. Discussion

4.1. The effect of precursors on framework and Cu species

SSZ-39 with the AEI topological structure contains D6R as basic units in the framework. Y zeolites also contain D6R, which do not occur in Beta or ZSM-5. The different basic units in Y, Beta and ZSM-5 lead to diverse assembly routes for SSZ-39 [17]. In this study, the Si/Al ratio of the Y zeolites is around 11, and the Si/Al ratio of the synthesized $Cu_{2.6}$-SSZ-39-Y is around 7.2. Meanwhile, the Si/Al ratio of Beta and

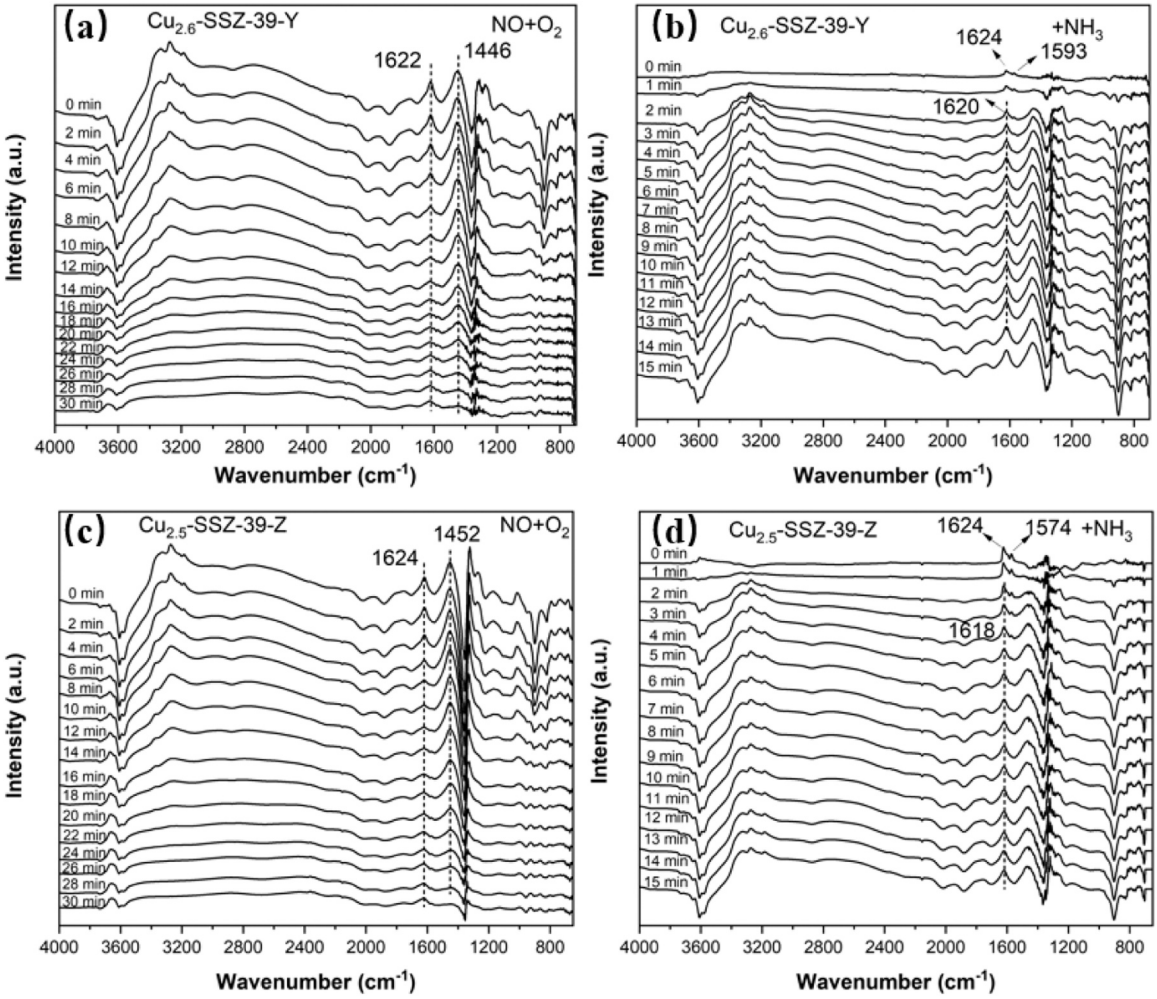

Fig. 9. *In situ* DRIFTS spectra of (a) $Cu_{2.6}$-SSZ-39-Y with NO and O_2 introduced after saturating by NH_3; (b) $Cu_{2.6}$-SSZ-39-Y with NH_3 introduced after saturating by NO and O_2; (c) $Cu_{2.5}$-SSZ-39-Z with NO and O_2 introduced after saturating by NH_3; (d) $Cu_{2.5}$-SSZ-39-Z with NH_3 inlet after saturating by NO and O_2.

ZSM-5 is around 12, and the synthesized $Cu_{2.6}$-SSZ-39-B and $Cu_{2.5}$-SSZ-39-Z have Si/Al ratios of 8.6 and 9.0, respectively. Compared with Y, higher atomic utilization was obtained when using Beta or ZSM-5 as precursor. Zhang et al. discussed the interzeolite transformation of Y, Beta and ZSM-5 to SSZ-39 zeolites. During the interzeolite transformation of Y to SSZ-39, Y firstly decomposed into double six-membered rings (D6R), and D6R assembled to form SSZ-39. However, besides D6R, there were also single four-membered rings (S4R) in Y zeolite, and these S4R cannot be utilized in the formation of AEI, thus the atomic utilization was low. When using ZSM-5 and Beta as precursors, single five-membered rings (S5R) were broken, and single six-membered rings (S6R) and S4R were left. These S6R and S4R assembled to form D6R which further form SSZ-39 zeolites. There was no useless primary constituent unit left when using ZSM-5 and Beta as precursors, thus their atomic utilizations were high. [17]. The initial Si/Al ratio of the synthesis gel is 60 when using colloidal silica and sodium aluminate as precursor, but the Si/Al of the synthesized $Cu_{2.5}$-SSZ-39-C is only 6.7. When using colloidal silica and sodium aluminate as precursors, multiple primary constituent units formed during the crystallization process. Some of the formed primary constituent units were useless, thus the atomic utilization of precursor became rather low. Therefore, using Beta and ZSM-5 as precursors, higher atomic utilization can be obtained, and the Si/Al ratio of the synthesized SSZ-39 is closer to that of the starting material.

The framework Si/Al ratio of Cu-SSZ-39 can affect the distribution of Cu species. When Si/Al is low, more paired-Al atoms exist in the framework, and Cu^{2+} species predominantly coordinate with paired-Al atoms. When the Si/Al ratio is high, more single Al atoms exist, providing ion-exchange sites for $Cu(OH)^+$ species [31]. Among the prepared Cu-SSZ-39 catalysts in this study, the framework Si/Al ratio follows the order: $Cu_{2.5}$-SSZ-39-Z > $Cu_{2.6}$-SSZ-39-B > $Cu_{2.6}$-SSZ-39-Y > $Cu_{2.5}$-SSZ-39-C. *In situ* DRIFTS of NH_3 adsorption results indicate that the amount of $Cu(OH)^+$ species follows the same order as the Si/Al ratio. $Cu(OH)^+$ species coordinate with single framework Al; thus, the interaction between $Cu(OH)^+$ species and framework Al is relatively weak. $Cu(OH)^+$ species possess better mobility, especially when NH_3 is present, facilitating low-temperature NH_3-SCR activity [32,33]. The NO_x conversion below 200 °C of the prepared catalysts follows the order: $Cu_{2.5}$-SSZ-39-Z > $Cu_{2.6}$-SSZ-39-B > $Cu_{2.6}$-SSZ-39-Y > $Cu_{2.5}$-SSZ-39-C, which is in accordance with the order the amount of $Cu(OH)^+$. To sum up, when using ZSM-5 to synthesize SSZ-39, the atomic utilization of the precursor is the highest. Meanwhile, owing to its relatively high Si/Al ratio, more $Cu(OH)^+$ species exist; thus, $Cu_{2.5}$-SSZ-39-Z shows the highest low-temperature NH_3-SCR activity.

4.2. Hydrothermal stability of the catalysts

The stability of the Cu species and framework determines the hydrothermal stability of zeolites. More specifically, the amount and form of Cu species and the framework Si/Al ratio are the main factors [47]. Cu^{2+} species coordinating with 2 framework Al atoms are relatively stable, while the stability of $Cu(OH)^+$ species coordinating with 1

framework Al atom is comparatively low [33,35]. Appropriate amounts of Cu ions can stabilize the framework through coordination. However, excessive amounts of Cu ions are prone to accumulate, and bulk Cu_xO_y species migrate among the pores of the zeolite, resulting in collapse of the framework [35]. Zeolites with low Si/Al ratio possess more ion-exchange sites which can hold more Cu ions and help to stabilize framework. Meanwhile, the Al atoms in the framework are charge defect sites, which are fragile under hydrothermal conditions. The framework of zeolites with high Si/Al ratio is more stable, but the amount of Cu ions they can hold is relatively low, and less stable $Cu(OH)^+$ species are likely to form. Overall, an appropriate amount of Cu ions and framework Si/Al ratio are necessary to obtain good hydrothermal stability for the catalyst [47].

In this study, the Cu/Al ratios of Cu-SSZ-39 catalysts prepared by different precursors are between 0.2 and 0.3. Under this range of Cu/Al ratios, Cu ions can protect the framework; meanwhile, they are not prone to accumulate [28]. Cu^{2+} and $Cu(OH)^+$ species possess different hydrothermal stabilities. As illustrated by H_2-TPR and *in situ* DRIFTS of NH_3 adsorption results, the number of $Cu(OH)^+$ species decreased evidently after hydrothermal aging, especially for $Cu_{2.6}$-SSZ-39-B and $Cu_{2.5}$-SSZ-39-Z. After hydrothermal aging at 900 °C, unlike $Cu_{2.5}$-SSZ-39-Z-HTA900, $Cu(OH)^+$ species in the other three catalysts vanished, with only a portion of the Cu^{2+} species being maintained in $Cu_{2.6}$-SSZ-39-B-HTA900. The decrease in SCR-active Cu ions led to a decrease in NH_3-SCR activity, but $Cu_{2.5}$-SSZ-39-Z-HTA900 still maintained high NO_x conversion.

Besides the loss of active Cu species, more notable changes were observed for the framework. After hydrothermal aging at 850 °C, different degrees of dealumination and decline in crystallinity occurred for the prepared catalysts. Comparatively, higher relative crystallinity was maintained in $Cu_{2.6}$-SSZ-39-B and $Cu_{2.5}$-SSZ-39-Z, which possess higher Si/Al ratios [21,22]. This result indicates that among the prepared Cu-SSZ-39 in this study, having fewer Al atoms in the framework is beneficial to the stability, which is more noticeable for hydrothermal aging at 900 °C. The XRD results indicated that $Cu_{2.6}$-SSZ-39-Y-HTA900 and $Cu_{2.5}$-SSZ-39-C-HTA900 completely lost crystallinity, and $Cu_{2.6}$-SSZ-39-B-HTA900 only maintained a faint diffraction peak around 9.7°. However, 82.8% crystallinity was still maintained in $Cu_{2.5}$-SSZ-39-Z-HTA900, which possesses the highest Si/Al ratio.

It is worth noting that the Si/Al ratio of $Cu_{2.6}$-SSZ-39-B and $Cu_{2.5}$-SSZ-39-Z is similar, but they behaved differently after hydrothermal aged at 900 °C. Besides, Si/Al ratio, other factors such as crystallite size, Al distribution and Cu distribution can also affect the hydrothermal of zeolites. As presented in Fig. 4, the particle sizes of the prepared catalysts are different with each other, and the grain of $Cu_{2.5}$-SSZ-39-Z is obviously larger than those of the other samples. Xu et al. and Liu et al. found that Cu-SAPO-34 and Cu-SSZ-13 with larger particle size possessed better hydrothermal stability, and it turned out that the distribution of Cu species and Al are the key factors [48,49]. XPS is a surface sensitive technology that can detect the elemental distribution on the surface of catalyst particles, and the atomic concentration on the surface of catalysts is presented in Table S1. The results indicated that less Cu and Al atoms locate on the surface of $Cu_{2.5}$-SSZ-39-Z, comparing with the other catalysts. Larger particle size of $Cu_{2.5}$-SSZ-39-Z results in more Cu and Al atoms being protected inside the particles. Therefore, the Cu and Al atoms in $Cu_{2.5}$-SSZ-39-Z are harder to be affected by H_2O in $Cu_{2.5}$-SSZ-39-Z during the hydrothermal aging process, and it behaved better after aging at 900 °C. In conclusion, besides larger Si/Al, larger particle size and less Cu & Al atoms on the surface also endowed the better hydrothermal stability of $Cu_{2.5}$-SSZ-39-Z.

5. Conclusion

In this study, Y zeolite, Beta zeolite, ZSM-5 zeolite, colloidal silica and sodium aluminate were used as precursors for the synthesis of Cu-SSZ-39. The catalysts prepared from different precursors presented good crystallinity and morphology. The Si/Al ratios of the prepared catalysts followed the order: $Cu_{2.5}$-SSZ-39-Z (9.0) > $Cu_{2.6}$-SSZ-39-B (8.6) > $Cu_{2.6}$-SSZ-39-Y (7.2) > $Cu_{2.5}$-SSZ-39-C (6.7). A high Si/Al ratio is beneficial to the formation of $Cu(OH)^+$ species, which is good for low-temperature NH_3-SCR activity. Therefore, the amount of $Cu(OH)^+$ species and level of NO_x conversion at low temperatures for the prepared catalysts followed the same order as the Si/Al ratio. *In situ* DRIFTS experiments indicated that more nitrate species prefer are generated on $Cu_{2.5}$-SSZ-39-Z than $Cu_{2.6}$-SSZ-39-Y; thus, $Cu_{2.5}$-SSZ-39-Z showed higher NO_x conversion at low temperatures.

Hydrothermal aging affects the zeolites from the aspects of Cu species and framework simultaneously. After hydrothermal aging at 850 °C, all of the prepared Cu-SSZ-39 catalysts showed decreases in the amounts of Cu ions and dealumination occurred, but $Cu_{2.5}$-SSZ-39-Z-HTA850 and $Cu_{2.6}$-SSZ-39-B-HTA850 with high Si/Al ratios retained more Cu ions and higher crystallinity. After hydrothermal aging at 900 °C, only $Cu_{2.5}$-SSZ-39-Z-HTA900, with the highest Si/Al ratio and the largest particle size, could retain good NH_3-SCR activity. The other three catalysts experienced serious dealumination and dramatic loss of active Cu species. In conclusion, the Cu-SSZ-39 catalyst prepared with ZSM-5 as precursor possessed both the best low-temperature SCR activity and the best hydrothermal stability. Considering that ZSM-5 is cheaper and more environmentally friendly than Y, the industrial preparation of Cu-SSZ-39 should give priority to using ZSM-5 as the precursor.

CRediT authorship contribution statement

Jinpeng Du: Data curation, Investigation, Formal analysis, Writing original draft, Writing - review & editing. **Shichao Han**: Data curation, Investigation, Validation. **Chi Huang**: Data curation, Investigation, Validation. **Yulong Shan**: Conceptualization, Methodology, Validation. **Yan Zhang**: Conceptualization, Methodology, Validation. **Wenpo Shan**: Conceptualization, Methodology, Validation, Writing - review & editing, Project administration. **Hong He**: Conceptualization, Writing - review & editing, Project administration, Resources, Supervision.

Declaration of Competing Interest

The authors declare that they have no known competing financial interests or personal relationships that could have appeared to influence the work reported in this paper.

Data Availability

Data will be made available on request.

Acknowledgments

This work was financially supported by the National Natural Science Foundation of China (52225004, 52200136, 51978640), the National Key Research and Development Program of China (2022YFC3704400), the Science and Technology Innovation “2025” major program in Ningbo (2020Z103) and the Construction Project of National New Material Production and Application Demonstration Platform (TC220H06N).

Additional information

Additional experimental procedures/data are provided in the Supplementary Information: XRD patterns prepared by ZSM-5, Y, colloidal silica and sodium aluminate of higher Si/Al ratio; N_2O concentration during NH_3-SCR tests; SO_2 resistance of the prepared catalysts; ^{29}Si NMR profiles; SEM images of catalysts aged at 850 °C and 900 °C; TEM images of catalysts aged at 900 °C; H_2-TPR curves of $Cu_{2.6}$-SSZ-39-B-A900 and $Cu_{2.6}$-SSZ-39-Z-A900 with baseline coincided; summary of relative Cu content derived from EPR spectra; acidity of catalysts derived form NH_3-

TPD profiles; time evolution of peak intensity of Lewis and Brønsted acid sites; atomic concentration of fresh and 900 °C aged catalysts.

Appendix A. Supporting information

Supplementary data associated with this article can be found in the online version at doi:10.1016/j.apcatb.2023.123072.

References

[1] D. Ding, J. Xing, S. Wang, Z. Dong, F. Zhang, S. Liu, J. Hao, Optimization of a NO_x and VOC cooperative control strategy based on clean air benefits, Environ. Sci. Technol. 56 (2022) 739–749.

[2] Y. Tan, P. Henderick, S. Yoon, J. Herner, T. Montes, K. Boriboonsomsin, K. Johnson, G. Scora, D. Sandez, T.D. Durbin, On-board sensor-based NO_x emissions from heavy-duty diesel vehicles, Environ. Sci. Technol. 53 (2019) 5504–5511.

[3] S. Jiang, T. Li, J. Zheng, H. Zhang, X. Li, T. Zhu, Unveiling the remarkable arsenic resistance origin of alumina promoted cerium-tungsten catalysts for NH_3-SCR, Environ. Sci. Technol. 54 (2020) 14740–14749.

[4] P. Li, Y. Xin, Q. Li, Z. Wang, Z. Zhang, L. Zheng, Ce-Ti amorphous oxides for selective catalytic reduction of NO with NH_3: confirmation of Ce-O-Ti active sites, Environ. Sci. Technol. 46 (2012) 9600–9605.

[5] D.W. Fickel, R.F. Lobo, Copper coordination in Cu-SSZ-13 and Cu-SSZ-16 investigated by variable-temperature XRD, J. Phys. Chem. C. 114 (2010) 1633–1640.

[6] M. Moliner, C. Franch, E. Palomares, M. Grill, A. Corma, Cu-SSZ-39, an active and hydrothermally stable catalyst for the selective catalytic reduction of NO_x, Chem. Commun. (Camb.) 48 (2012) 8264–8266.

[7] D.W. Fickel, E. D'Addio, J.A. Lauterbach, R.F. Lobo, The ammonia selective catalytic reduction activity of copper-exchanged small-pore zeolites, Appl. Catal. B: Environ. 102 (2011) 441–448.

[8] J.H. Kwak, R.G. Tonkyn, D.H. Kim, J. Szanyi, C.H.F. Peden, Excellent activity and selectivity of Cu-SSZ-13 in the selective catalytic reduction of NO_x with NH_3, J. Catal. 275 (2010) 187–190.

[9] S. Han, L. Wang, Y. Ma, W. Chen, Q. Wu, L. Zhang, Q. Zhu, X. Meng, A. Zheng, F. Xiao, Potassium-directed sustainable synthesis of new high silica small-pore zeolite with KFI structure (ZJM-7) as an efficient catalyst for NH_3-SCR reaction, Appl. Catal. B: Environ. 281 (2021) 119480–119487.

[10] D. Jo, T. Ryu, G.T. Park, P.S. Kim, C.H. Kim, I.-S. Nam, S.B. Hong, Synthesis of high-silica LTA and UFI zeolites and NH_3–SCR performance of their copper-exchanged form, ACS Catal. 6 (2016) 2443–2447.

[11] T. Ryu, N.H. Ahn, S. Seo, J. Cho, H. Kim, D. Jo, G.T. Park, P.S. Kim, C.H. Kim, E. L. Bruce, P.A. Wright, I.S. Nam, S.B. Hong, Fully copper-exchanged high-silica LTA zeolites as unrivaled hydrothermally stable NH_3-SCR catalysts, Angew. Chem. Int. Ed. Engl. 56 (2017) 3256–3260.

[12] Q. Lin, S. Xu, H. Zhao, S. Liu, H. Xu, Y. Dan, Y. Chen, Highlights on key roles of Y on the hydrothermal stability at 900 °C of Cu/SSZ-39 for NH_3-SCR, ACS Catal. 12 (2022) 14026–14039.

[13] N. Martin, C.R. Boruntea, M. Moliner, A. Corma, Efficient synthesis of the Cu-SSZ-39 catalyst for $DeNO_x$ applications, Chem. Commun. (Camb.) 51 (2015) 11030–11033.

[14] M. Dusselier, R. Moulton, B. Haymore, M. Hellums, M.E. Davis, Influence of organic structure directing agent isomer distribution on the synthesis of SSZ-39, Chem. Mater. 27 (2015) 2695–2702.

[15] H. Xu, W. Chen, Q. Wu, C. Lei, J. Zhang, S. Han, L. Zhang, Q. Zhu, X. Meng, D. Dai, S. Maurer, A.-N. Parvulescu, U. Müller, W. Zhang, T. Yokoi, X. Bao, B. Marler, D. E. De Vos, U. Kolb, A. Zheng, F. Xiao, Transformation synthesis of aluminosilicate SSZ-39 zeolite from ZSM-5 and beta zeolite, J. Mater. Chem. A 7 (2019) 4420–4425.

[16] H. Xu, J. Zhang, Q. Wu, W. Chen, C. Lei, Q. Zhu, S. Han, J. Fei, A. Zheng, L. Zhu, X. Meng, S. Maurer, D. Dai, A.N. Parvulescu, U. Muller, F. Xiao, Direct synthesis of aluminosilicate SSZ-39 zeolite using colloidal silica as a starting source, Acs. Appl. Mater. Interfaces 11 (2019) 23112–23117.

[17] J. Zhang, Y. Chu, F. Deng, Z. Feng, X. Meng, F. Xiao, Evolution of D6R units in the interzeolite transformation from FAU, MFI or *BEA into AEI: transfer or reassembly? Inorg. Chem. Front. 7 (2020) 2204–2211.

[18] J. Du, Y. Shan, G. Xu, Y. Sun, Y. Wang, Y. Yu, W. Shan, H. He, Effects of SO_2 on Cu-SSZ-39 catalyst for the selective catalytic reduction of NO_x with NH_3, Catal. Sci. Technol. 10 (2020) 1256–1263.

[19] T. Sonoda, T. Maruo, Y. Yamasaki, N. Tsunoji, Y. Takamitsu, M. Sadakane, T. Sano, Synthesis of high-silica AEI zeolites with enhanced thermal stability by hydrothermal conversion of FAU zeolites, and their activity in the selective catalytic reduction of NO_x with NH_3, J. Mater. Chem. A 3 (2015) 857–865.

[20] J. Du, Y. Shan, Y. Sun, M. Gao, Z. Liu, X. Shi, Y. Yu, H. He, Unexpected increase in low-temperature NH_3-SCR catalytic activity over Cu-SSZ-39 after hydrothermal aging, Appl. Catal. B: Environ. 294 (2021) 120237–120246.

[21] A.M. Beale, F. Gao, I. Lezcano-Gonzalez, C.H. Peden, J. Szanyi, Recent advances in automotive catalysis for NO_x emission control by small-pore microporous materials, Chem. Soc. Rev. 44 (2015) 7371–7405.

[22] C. Fan, Z. Chen, L. Pang, S. Ming, X. Zhang, K.B. Albert, P. Liu, H. Chen, T. Li, The influence of Si/Al ratio on the catalytic property and hydrothermal stability of Cu-SSZ-13 catalysts for NH_3-SCR, Appl. Catal. A: Gen. 550 (2018) 256–265.

[23] R. Li, Y. Zhu, Z. Zhang, C. Zhang, G. Fu, X. Yi, Q. Huang, F. Yang, W. Liang, A. Zheng, J. Jiang, Remarkable performance of selective catalytic reduction of NO_x by ammonia over copper-exchanged SSZ-52 catalysts, Appl. Catal. B: Environ. 283 (2021).

[24] R. Osuga, T. Takeuchi, M. Sawada, Y. Kunitake, T. Matsumoto, S. Yasuda, H. Onozuka, S. Tsutsuminai, J.N. Kondo, H. Gies, T. Yokoi, Fabrication of AEI-type aluminosilicate with sheet-like morphology for direct conversion of propene to butenes, Catal. Sci. Technol. 11 (2021) 5839–5848.

[25] X. Yong, C. Zhang, M. Wei, P. Xie, Y. Li, Promotion of the performance of Cu-SSZ-13 for selective catalytic reduction of NO_x by ammonia in the presence of SO_2 during high temperature hydrothermal aging, J. Catal. 394 (2021) 228–235.

[26] J. Zhu, Z. Liu, L. Xu, T. Ohnishi, Y. Yanaba, M. Ogura, T. Wakihara, T. Okubo, Understanding the high hydrothermal stability and NH_3-SCR activity of the fast-synthesized ERI zeolite, J. Catal. 391 (2020) 346–356.

[27] H. Tian, Y. Ping, Y. Zhang, Z. Zhang, L. Sun, P. Liu, J. Zhu, X. Yang, Atomic layer deposition of silica to improve the high-temperature hydrothermal stability of Cu-SSZ-13 for NH_3 SCR of NO_x, J. Haz. Mat. 416 (2021) 126194–126203.

[28] Y. Shan, J. Du, Y. Yu, W. Shan, X. Shi, H. He, Precise control of post-treatment significantly increases hydrothermal stability of in-situ synthesized cu-zeolites for NH_3-SCR reaction, Appl. Catal. B: Environ. 266 (2020) 118655–118666.

[29] J. Hun Kwak, H. Zhu, J.H. Lee, C.H. Peden, J. Szanyi, Two different cationic positions in Cu-SSZ-13? Chem. Commun. (Camb.) 48 (2012) 4758–4760.

[30] F. Gao, E.D. Walter, E.M. Karp, J. Luo, R.G. Tonkyn, J.H. Kwak, J. Szanyi, C.H. F. Peden, Structure–activity relationships in NH_3-SCR over Cu-SSZ-13 as probed by reaction kinetics and EPR studies, J. Catal. 300 (2013) 20–29.

[31] C. Paolucci, A.A. Parekh, I. Khurana, J.R. Di Iorio, H. Li, J.D. Albarracin Caballero, A.J. Shih, T. Anggara, W.N. Delgass, J.T. Miller, F.H. Ribeiro, R. Gounder, W. F. Schneider, Catalysis in a cage: condition-dependent speciation and dynamics of exchanged Cu cations in SSZ-13 zeolites, J. Am. Chem. Soc. 138 (2016) 6028–6048.

[32] A.M. Beale, I. Lezcano-Gonzalez, W.A. Slawinski, W.A. Slawinksi, D.S. Wragg, correlation between Cu ion migration behaviour and $deNO_x$ activity in Cu-SSZ-13 for the standard NH_3-SCR reaction, Chem. Commun. (Camb.) 52 (2016) 6170–6173.

[33] J. Zhang, Y. Shan, L. Zhang, J. Du, H. He, S. Han, C. Lei, S. Wang, W. Fan, Z. Feng, X. Liu, X. Meng, F. Xiao, Importance of controllable Al sites in CHA framework by crystallization pathways for NH_3-SCR reaction, Appl. Catal. B: Environ. 277 (2020) 119193–119200.

[34] Y. Ma, S. Cheng, L. Cao, L. Liu, Y. Xu, J. Liu, R. Ran, Z. Si, D. Weng, Relationships between copper speciation and Brønsted acidity evolution over Cu-SSZ-13 during hydrothermal aging, Appl. Catal. A: Gen. 602 (2020) 117650–117661.

[35] Y.J. Kim, J.K. Lee, K.M. Min, S.B. Hong, I.-S. Nam, B.K. Cho, Hydrothermal stability of CuSSZ13 for reducing NO_x by NH_3, J. Catal. 311 (2014) 447–457.

[36] S. Han, Q. Ye, S. Cheng, T. Kang, H. Dai, Effect of the hydrothermal aging temperature and Cu/Al ratio on the hydrothermal stability of CuSSZ-13 catalysts for NH_3-SCR, Catal. Sci. Technol. 7 (2017) 703–717.

[37] Y. Shan, W. Shan, X. Shi, J. Du, Y. Yu, H. He, A comparative study of the activity and hydrothermal stability of Al-rich Cu-SSZ-39 and Cu-SSZ-13, Appl. Catal. B: Environ. 264 (2020) 118511–118520.

[38] D. Wang, F. Gao, C.H.F. Peden, J. Li, K. Kamasamudram, W.S. Epling, Selective catalytic reduction of NO_x with NH_3 over a Cu-SSZ-13 catalyst prepared by a solid-state ion-exchange method, ChemCatChem 6 (2014) 1579–1583.

[39] D. Wang, L. Zhang, J. Li, K. Kamasamudram, W.S. Epling, NH_3-SCR over Cu/SAPO-34 – zeolite acidity and Cu structure changes as a function of Cu loading, Catal. Today 231 (2014) 64–74.

[40] A. Wang, L. Olsson, Insight into the SO_2 poisoning mechanism for NO_x removal by NH_3-SCR over Cu/LTA and Cu/SSZ-13, Chem. Engin. J. 395 (2020) 125048–125059.

[41] J. Luo, F. Gao, K. Kamasamudram, N. Currier, C.H.F. Peden, A. Yezerets, New insights into Cu/SSZ-13 SCR catalyst acidity. Part I: Nature of acidic sites probed by NH_3 titration, J. Catal. 348 (2017) 291–299.

[42] R. Li, X. Jiang, J. Lin, Z. Zhang, Q. Huang, G. Fu, Y. Zhu, J. Jiang, Understanding the influence of hydrothermal treatment on NH_3-SCR of NO activity over Cu -SSZ-16, Chem. Engin. J. 441 (2022) 136021–136030.

[43] C. Paolucci, J.R. Di Iorio, F.H. Ribeiro, R. Gounder, W.F. Schneider, Catalysis science of NO_x selective catalytic reduction with ammonia over Cu-SSZ-13 and Cu-SAPO-34, Adv. Catal. 59 (2016) 1–107.

[44] D. Wang, L. Zhang, K. Kamasamudram, W.S. Epling, In situ-DRIFTS study of selective catalytic reduction of NO_x by NH_3 over Cu-exchanged SAPO-34, ACS Catal. 3 (2013) 871–881.

[45] Y. Mao, H. Wang, P. Hu, Theoretical Investigation of NH_3-SCR processes over zeolites: a review, Int. J. Quantum Chem. 115 (2015) 618–630.

[46] Y. Zhang, Y. Peng, K. Li, S. Liu, J. Chen, J. Li, F. Gao, C.H.F. Peden, Using transient FTIR spectroscopy to probe active sites and reaction intermediates for selective catalytic reduction of NO on Cu/SSZ-13 catalysts, ACS Catal. 9 (2019) 6137–6145.

[47] Y. Shan, J. Du, Y. Zhang, W. Shan, X. Shi, Y. Yu, R. Zhang, X. Meng, F. Xiao, H. He, Selective catalytic reduction of NO_x with NH_3: opportunities and challenges of Cu-based small-pore zeolites, Natl. Sci. Rev. 8 (2021) nwab010.

[48] H. Xu, C. Lin, Q. Lin, X. Feng, Z. Zhang, Y. Wang, Y. Chen, Grain size effect on the high-temperature hydrothermal stability of Cu/SAPO-34 catalysts for NH_3-SCR, J. Environ. Chem. Eng. 8 (2020) 104559–104566.

[49] H. Liu, M. Shen, C. Wang, J. Wang, J. Wang, G. Shen, Revealing the effect of crystal size on the high-temperature hydrothermal stability of Cu/SSZ-13 NH_3-SCR catalysts, Catal. Sci. Technol. 13 (2023) 3579–3589.